# CHARACTERIZING AND INTEGRATING RESISTIVE INK FOR USE IN RF COMPONENTS

By

Koltin Grammer

#### A THESIS

Submitted to
Michigan State University
in partial fulfillment of the requirements
for the degree of

Electrical and Computer Engineering – Master of Science

2025

#### **ABSTRACT**

Aerosol jet printing (AJP) is gaining attention in additive manufacturing as a method that can be used to fabricate small and precise radio frequency (RF) components. Although work has been done to prove the usefulness of this manufacturing method up to D-band, most of that work has been done using highly conductive inks for transmission lines and radiators. Currently, no reliable method exists to fabricate resistive components for use in high-frequency circuits. The work presented here undergoes the process of characterizing commercially available ink for that purpose. It will be shown that resistors can be fabricated small enough and with low enough resistance to be used in RF components. A Wilkinson power divider that operates in Ka band as well as one that operates in V band are fabricated. A set of loaded microstrips are fabricated to show how the printed resistors operate when they act as terminations.

This thesis is dedicated to my wife Emily.

Thank you for the unwavering support from the beginning.

### **ACKNOWLEDGEMENTS**

This work is funded in part by the Department of Energy's Kansas City National Security Campus, operated by Honeywell Federal Manufacturing & Technologies, LLC under contract number DE-NA0002839.

### TABLE OF CONTENTS

•===== = ==== · · · · · · · · · · · · ·	
1.1 Aerosol Jet Printing	
1.2 How AJP Works	
CHAPTER 2: Ink Selection	6
2.1 Clevious FE T	6
2.2 Mixed Materials	15
2.3 Metalon JR-038	
CHAPTER 3: Characterizing Metalon Resistive Ink	17
CILIT 121 01 CHAILACOTTEMS INTOMICAL TROUBUSE (C. 1111)	
CHAPTER 4: Fabricating RF Devices	25
	25 25
CHAPTER 4: Fabricating RF Devices  4.1 Load Terminated Microstrip  4.2 Wilkinson Power Divider	
CHAPTER 4: Fabricating RF Devices 4.1 Load Terminated Microstrip 4.2 Wilkinson Power Divider  CHAPTER 5: Conclusions and Future Work	
CHAPTER 4: Fabricating RF Devices 4.1 Load Terminated Microstrip 4.2 Wilkinson Power Divider  CHAPTER 5: Conclusions and Future Work 5.1 Altering Ink Resistivity	
CHAPTER 4: Fabricating RF Devices 4.1 Load Terminated Microstrip 4.2 Wilkinson Power Divider  CHAPTER 5: Conclusions and Future Work	

# **CHAPTER 1: Introduction**

#### 1.1 Aerosol Jet Printing

The rapid proliferation of radio frequency (RF) components calls for advanced manufacturing techniques that are capable of high precision fabrication, miniaturization, and customization. One such technique is aerosol jet printing (AJP). AJP stands out for its ability to print over a wide range of length scales, with previous work showing its ability to print down to 10µm [1], [2], as well as its ability to print functional components in Ka, W, and D band [3], [4], [2]. AJP is an additive process, unlike many of the currently utilized processes, which are subtractive in nature and therefore generate significant amounts of material waste and dangerous chemical waste (hydrofluoric acid). The current semiconductor processes require mask fabrication and lithography, where the AJP process can quickly customize designs and adjust fine feature sizes as needed leading to a reduction in non-reoccurring engineering (NRE). AJP has proven successful in the field of packaging with its ability to print broadband, low-loss interconnects [5]. Additionally, AJP as the ability to print over conformal surfaces [4], as well as across multiple layers [6].

While previous work has shown the utility of AJP, little research has gone into using this manufacturing technique to fabricate structures other than dielectrics (polyimide, benzocyclobutene) or conductors (silver). The few attempts at fabricating resistive components have produced components that were either too resistive [7], too large [8], or required extremely high levels of process control relative to the methods shown in this thesis [7], [8], [9]. RF devices typically require resistive components that have relatively low resistive values ( $100\Omega$  for Wilkinson power divider). RF devices require resistive components to be much smaller than a

wavelength to be considered lumped (one-sixth being a rule of thumb [10]), and high levels of process control can make resistor fabrication and repeatability difficult.

The work in this thesis will explore various resistive ink options and rule out less desirable inks. It will be shown possible to print resistors that are physically small, relatively low resistance, and repeatable using a commercially available carbon-based ink. The characterization process will show how to fabricate resistors of a given size and resistance as well as how curing effects device geometry. The I-V characteristics of the fabricated resistor will show that the resistor has ohmic behavior. Finally, RF devices will be fabricated using the printed resistor to prove their effectiveness in actual components.

#### 1.2 How AJP Works



Figure 1.1: Aerosol jet printer at Michigan State University

Aerosol jet printing is a direct writing method and happens in four basic stages: ink preparation, ink atomization and transport, ink deposition, and post processing.

During the ink preparation stage, the material that is to be printed may need to be altered

to be compatible with the printer. The most important aspect is the ink viscosity. If the material is too viscous, it will not be able to be atomized and transported to the deposition stage. Both the polyimide and the silver that are used to fabricate the RF devices in chapter 4 are altered during the ink preparation stage. The carbon ink that is used to fabricate the resistor does not require any ink preparation.

Two methods are used for ink atomization: pneumatic atomization (PA) and ultrasonic atomization (UA). PA is typically used for more viscous inks, such as the polyimide used to form the dielectric layers. UA is used for less viscous ink such as silver, and carbon.

During pneumatic atomization nitrogen enters the system though the atomizer inlet gas nozzle at the top of the pneumatic atomizer and is directed into the jar. Inside the bottom of the jar is a jet that directs the nitrogen into the jar and atomizes the ink. The difference in pressure then carries the nitrogen-ink mixture to the mist output port. The exhaust is in line with the mist output and removes access air from the system. A pictorial representation of the pneumatic atomizer is given in figure 1.2.

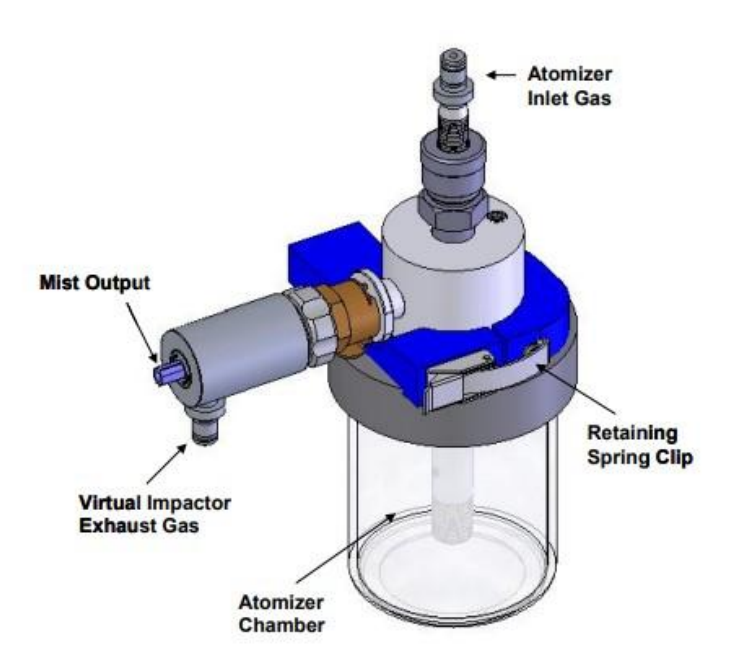


Figure 1.2: Pneumatic atomizer [11]

Ultrasonic atomization operates in a similar fashion; however, the vial of ink is suspended in a water bath that has a transducer at the bottom. The transducer vibrates the water which transfers the vibration into the ink resulting in a small amount of ink atomization.

Nitrogen enters the system and carries away the ink droplets. There is no exhaust during ultrasonic atomization.

The deposition head is the same for both PA and UA. The nitrogen-ink mixture is delivered to the deposition head that uses a nitrogen sheath gas to focus the mixture into a focused stream prior to leaving the system. Once the ink leaves the system it is deposited onto the print stage where the part is being fabricated. To temporarily stop deposition during this process a shutter is used to temporarily cover the nozzle when needed. A pictorial representation of the deposition head is given in figure 1.3.

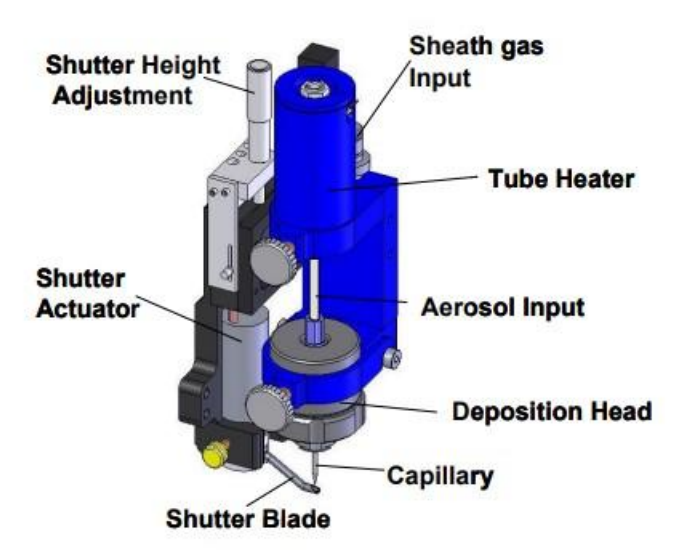


Figure 1.3: Deposition head [11]

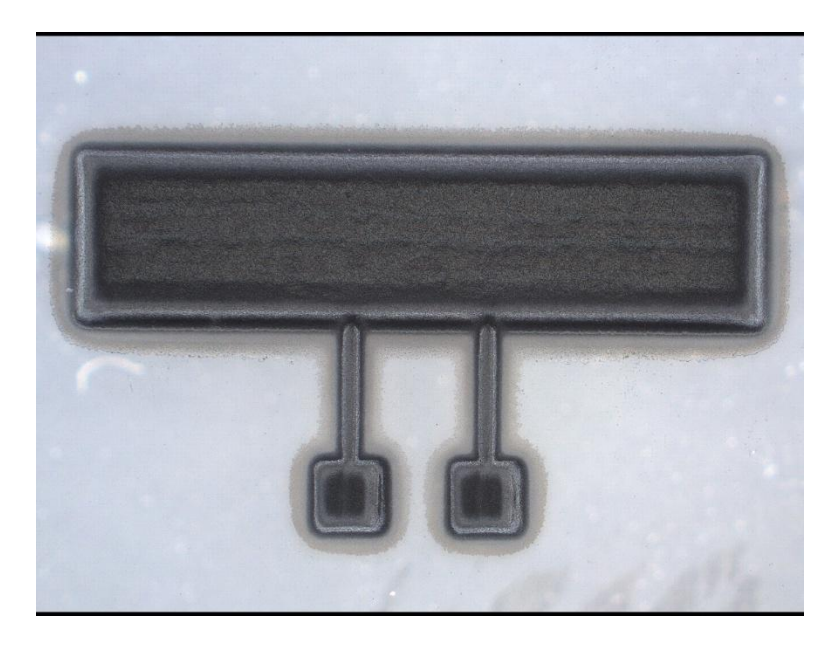
The post processing step is dependent on the material that was being printed. Silver and carbon undergo cures in an oven with no change in atmosphere. Polyimide undergoes cure in a vacuum oven with atmosphere pumped out and nitrogen pumped in. Some inks are cured using ultra-violet (UV) light, but none of those were used in this work.

# **CHAPTER 2: Ink Selection**

#### 2.1 Clevious FE T

The first ink evaluated was Clevious FE T, manufactured by Heraeus. This ink is a Poly(3,4-ethylenedioxythiophene) polystyrene sulfonate (PEDOT: PSS) based mixture. The PEDOT component of this mixture contributes to its electrical conductivity. The sulfonate component contributes to water solubility. This mixture has a reported sheet resistance range of  $80-500 \frac{\Omega}{sq}$  [12], which could make it an ideal candidate for resistor fabrication. Additionally, some groups have had success using aerosol jet printing with this ink to print ultra-wide band RF components [13]; However, the characterization and printing procedure was not explored in detail. PEDOT: PSS mixtures have also been used in the ink-jet printing process [14], [15], [16]. In [14] the authors used a mixture of ink-jetting and capillary channels to control the deposition of the PEDOT: PSS ink. In [16] patterning was used to control the deposition. While these methods are valid, they require a significant amount of preparation and pre-processing of the print area. The goal of this thesis is to discover a method that eliminates those pre-processing steps and only utilizes AJP.

The Clevious FE T has a reported viscosity of 50-70 mPA-s [12]. Due to its viscosity, the pneumatic atomizer was used to print resistive test structures. These test structures would be used not only to test its electrical capabilities but determine also how it reacted mechanically to the print and curing process. The printed test structure is given in figure 2.1.



(a)

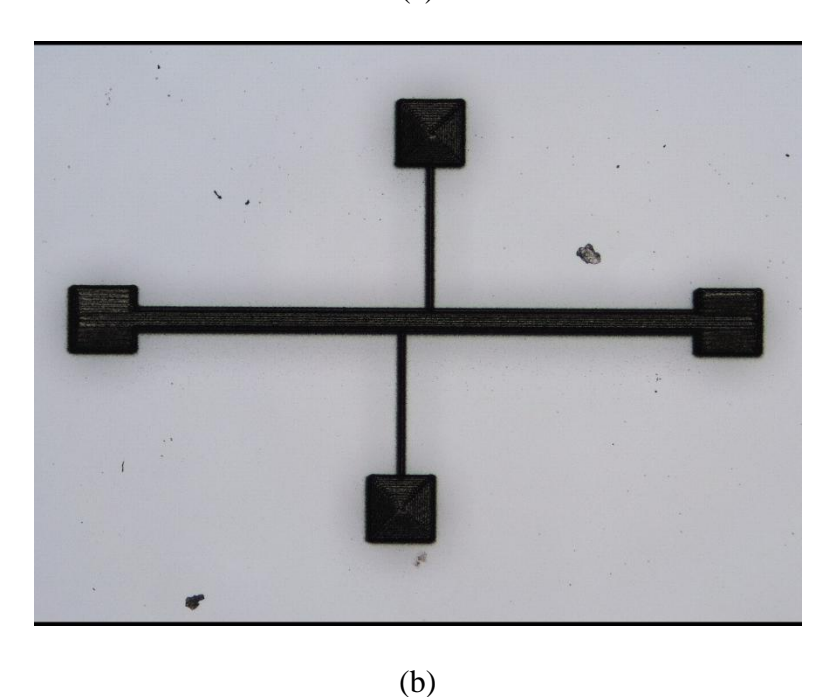


Figure 2.1: Two different test structures: (a) 1.5mm x 1mm (b) 100μm x 100μm

The test structures were printed using the following recipe: 1000 standard cubic centimeters per minute (SCCM) PA mass flow rate, 850 SCCM exhaust flow rate, tip speed 2 mm/s and 300µm tip. The curing profile was 100°C for 30 minutes in accordance with [12]. While the initially printed test structures looked promising, problems with the curing profile

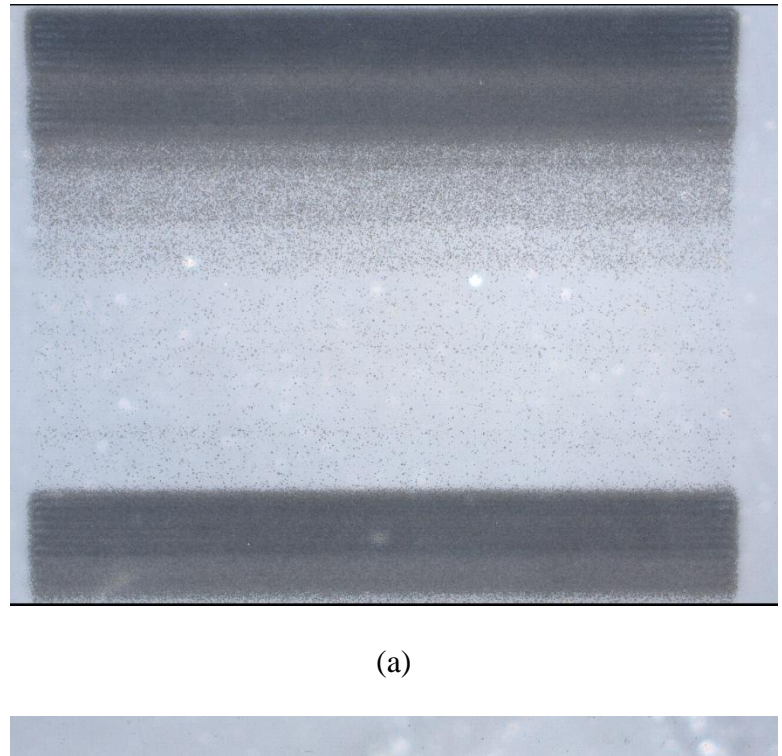
were immediately evident. Table 2.1 gives the height of the test structures before cure and after cure.

Table 2.1: Shrinkage profile of Clevious devices

Before Cure Height (µm)	After Cure Height (µm)	Shrinkage (%)
13.07	5.53	58
18.42	5.90	68
30.88	6.83	78
41.22	6.18	85
55.14	11.36	79
148.90	34.49	77
132.80	45.87	65
179.66	35.83	80
152.70	35025	77

The largest change in the height from pre-cure to post-cure was an 85% change in structure height. The reported change in structure height given in [12] is greater than 98%, therefore, the material was not reacting mechanically as expected.

Figure 2.2 shows two attempted prints that were fading in and out during deposition. This problem was prolonged and extended across numerous attempts to print simple square structures. While investigating the cause behind the fading prints, it was discovered that the ink reacted poorly to the AJP process. The ink was clogging the printer machinery during the process. some of the clogging examples are given in figure 2.3.



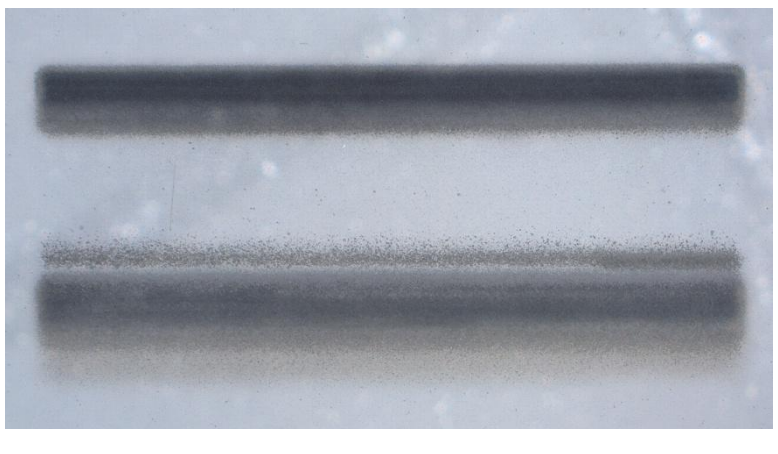


Figure 2.2: Continuous prints that fade during printing

(b)





Figure 2.3: Clevious FE T drying out in machinery parts during printing

Figure 2.3 shows that the ink drying out inside the printer's virtual impactor during the printing process. The nitrogen flow that carries the ink from the PA to the deposition nozzle was most likely flashing off the solvents in the ink. This led to poor print consistency and would make fabricating a given geometry difficult. This drying is also likely a cause for the poor shrinkage performance during the cure. Less solvents remain in the ink when deposited, therefore, there is less solvent to flash off during the cure and as a result, less shrinkage occurs. This was tested and verified by using a dropper to drop the ink onto a glass slide and measuring the pre-cure and post-cure height. This experiment results in a curing profile that was closer to that reported in the data sheet but would make it impossible to reliably fabricate resistors of a predetermined geometry without significant preparation.

To make matters worse, similar issues were discovered inside the PA print jar that holds the ink during print. Inside the jar is a metal ball that is used to slowly stir the ink while the machine is in operation. The ink is very acidic, and the ions in the ink tend to react with the metal. This reaction can change the ink chemical properties as well as cause the ink to congeal inside the jar. This issue was discovered when cleaning the ink jar to correct the fading print issues. Proof of the congealed ink is given in figure 2.4.



(a)



Figure 2.4: (a) Congealed ink in PA jar. (b) Result of filtering ink (c)Ink congealing around metal stir ball

Figure 2.4 (cont'd)



When testing the electrical characteristics of the few successfully printed structures, the Clevious could finally be eliminated as a candidate for an ink that could be used reliability. The I-V characteristics of the structure did not show consistent ohmic behavior but rather showed evidence of non-linear behavior. The I-V characteristics of the printed test structure are given in figure 2.5.

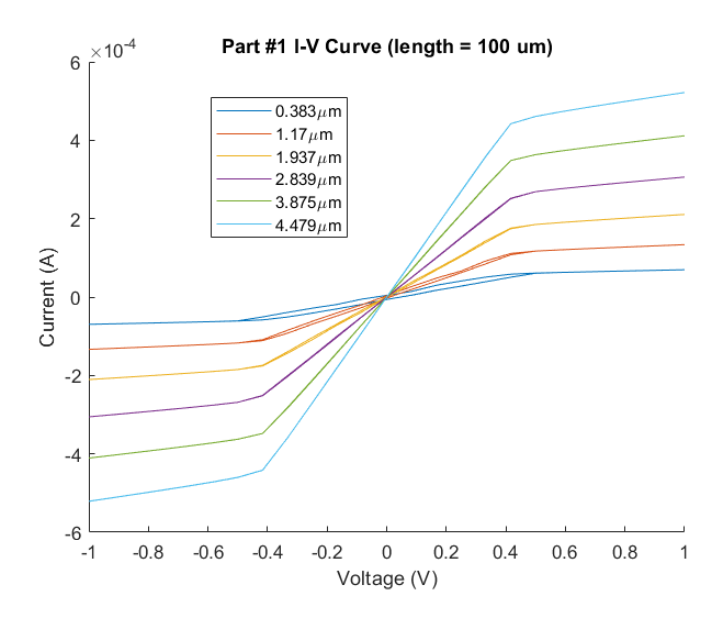


Figure 2.5: Test structure I-V characteristics (100µm x 100µm structure) with varying height

Over the range from -1 to 1 volt, the current does not increase linearly. The curve is linear when less than -0.4 volts, between -0.4 and 0.4 volts, and above 0.4 volts; however, the slope of these regions is not consistent. This behavior was repeated with similar results but with the diode behavior starting and stopping at different points based on test structure geometry. Figure 2.6 shows another test of the same nature but on different test structures that are significantly larger.

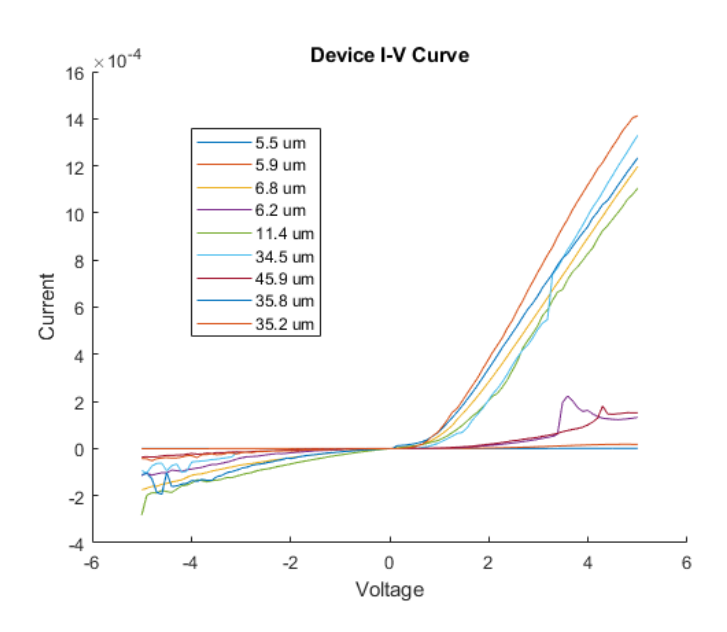


Figure 2.6: Test structure I-V characteristics (1.5mm x 1mm test structure)

Some tests were done that involved mixing additional solvents in with the ink prior to printing. It has been reported that mixing in solvents can help lower the resistivity of the ink [17]. It was possible that loading in additional solvents could help counterbalance the jamming issue by giving a larger buffer for solvent evaporation in the printer. These methods were attempted; however, were ultimately unsuccessful.

For the above reasons, Clevious ink was ruled out as a reliable candidate for AJP resistor printing applications.

#### 2.2 Mixed Materials

The work presented in [5] shows that it is possible to mix a highly conductive ink (silver) with other less conductive inks (graphene, carbon nanotubes, and carbon black nanoparticles). This work utilized both the pneumatic and ultrasonic atomizers simultaneously to mix ink in process. The ratio of carbon materials to silver was varied from 0% to 1% The resulting change in resistivity varied from roughly  $10^{-5} \Omega$ -cm to  $10 \Omega$ -cm. While this range would include resistivity values that would be useful for small RF components, there is a range that is six orders of magnitude within an exceedingly small change in carbon content. The inks were mixed during the printing process using a "Y" type connector that connected both the PA and UA. Process drift could make achieving a small variance in resistance for a given device difficult without high levels of process controls.

Opting to mix carbon nanotubes with various solvents prior to use in the UA was attempted in [7]. This removes some of the difficulty associated with process drift and controlling two different printer flows. Instead that high degree of process control is needed in the form of weighing inks and mixing with high degrees of precision. Ensuring a uniform mixture of carbon to solvents is important. To mitigate that issue a centrifuge was used. This would require specialized equipment and could still prove difficult to have a low variance in resistor values for a given device.

Resistive carbon paste can be diluted to meet the viscosity requirements of AJP. It was shown that this diluted carbon paste solution can successfully print resistors [8]. The resistors printed in [8] were small enough to use for low frequency RF applications, so continuation of this work could have proved fruitful; however, this process involves precisely diluting highly viscous carbon paste to create a solution that can be printed, and this is an added layer of

difficulty beyond printing. The paste used in [8] is manufactured for screen printing and it was noted in [8] that the particle size could lead to problems when using this method for AJP.

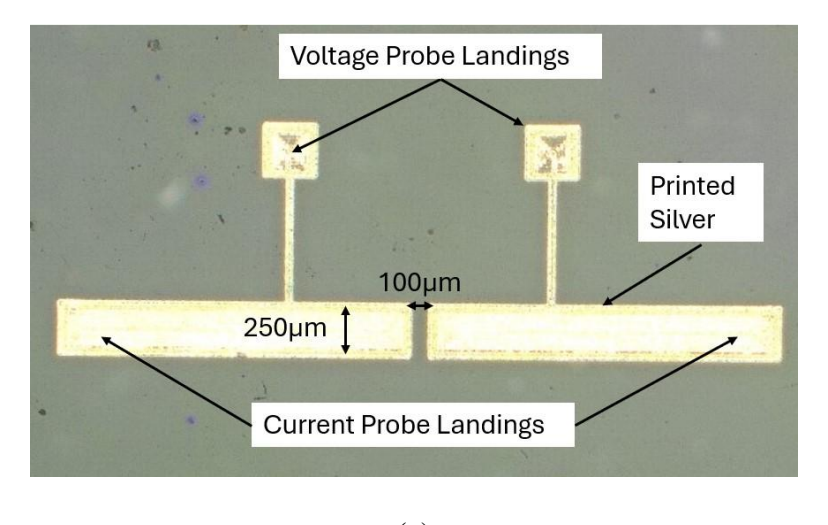
It is for the reasons above that diluting carbon paste to formulate a new ink was ruled out as a candidate for AJP resistor printing.

#### 2.3 Metalon JR-038

The ink that was chosen for characterization and device fabrication is Metalon JR-038 manufactured by Novacentrix. This ink is designed specifically for use in the AJP process and can be printed onto both porous (polyimide) and non-porous (glass) substrates. The ink has a reported resistivity of  $8000~\Omega$ - $\mu$ m [18]. During the initial testing, this ink proved to be easy to print, had reliable resistivity values, and did not require any pre-processing.

# **CHAPTER 3: Characterizing Metalon Resistive Ink**

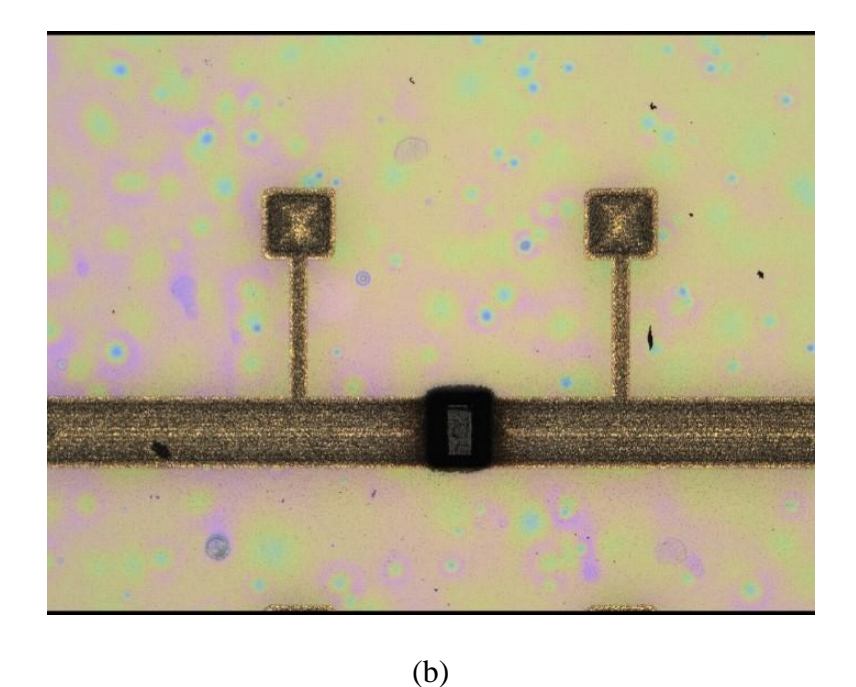
The end goal of the resistive ink is for use in various RF components which are normally mounted on a dielectric substrate, therefore, to best match the final mounting environment during testing, a glass slide (3"x2") was spin coated with the same polyimide that would be used in component fabrication. This layer of polyimide will provide a surface for Metalon ink to adhere to, substantially lowering the potential for delamination. A silver test structure was designed that would provide area for the resistor as well as provide convenient probe landing locations. The printed resistor would be placed in a gap between the two halves of the silver. This makes it possible to vary resistor length by adjusting the size of gap. The gap was made the same size as the gap that would be needed for a Wilkinson power divider that operates in Ka band. The gap was made 100µm long (space between silver) and 250µm wide. The test structure with and without the resistive ink is given in Fig 3.1.



(a)

Figure 3.1: Resistor test structures

Figure 3.1 (cont'd)



This test setup will also ensure that any resistance at the interface between the silver and the carbon will be included in any measurements that are taken, assuming the amount of overlap between the two materials remains constant. The overlapping region is important to the operation of the device, most importantly, the amount of overlap that exists. If the overlap is too low, then the I-V characteristics of the resistors can be unpredictable, likely due to the weak connection between the materials. It was found that an overlap of 40µm was sufficient for this application;

Sixteen test structures, including the resistor, were fabricated utilizing the  $40\mu m$  carbon-silver overlap. The print recipe was as follows: 75 standard cubic centimeters per minute (SCCM) sheath flow, 25 SCCM ultrasonic atomizer flow, 200 $\mu m$  tip, and 1  $\frac{mm}{s}$  tip speed. The resistors were cured at 100°C for 30 minutes. The resistors were printed to an arbitrary height and the cross-sectional area of the printed resistor would be measured using a Keyence optical profilometer, therefore, all geometric properties of the resistor will be known. The I-V

however, no detailed studies were done to prove that there is anything unique about this value.

characteristics of the resistor were measured using a four-point probe. Determining the resistivity of the material (after cure) is then possible using the relationship given in equation 3.1. With the resistivity of the material known, it could be possible to tailor the resistor values and geometry to the needs of the application.

$$R = \rho \frac{length}{cross - sectional\ area} \tag{3.1}$$

The resistivity value cited for this curing profile is  $8000\Omega$  -  $\mu m$  [18]. The resistivity values that were measured and calculated are given in figure 3.2.

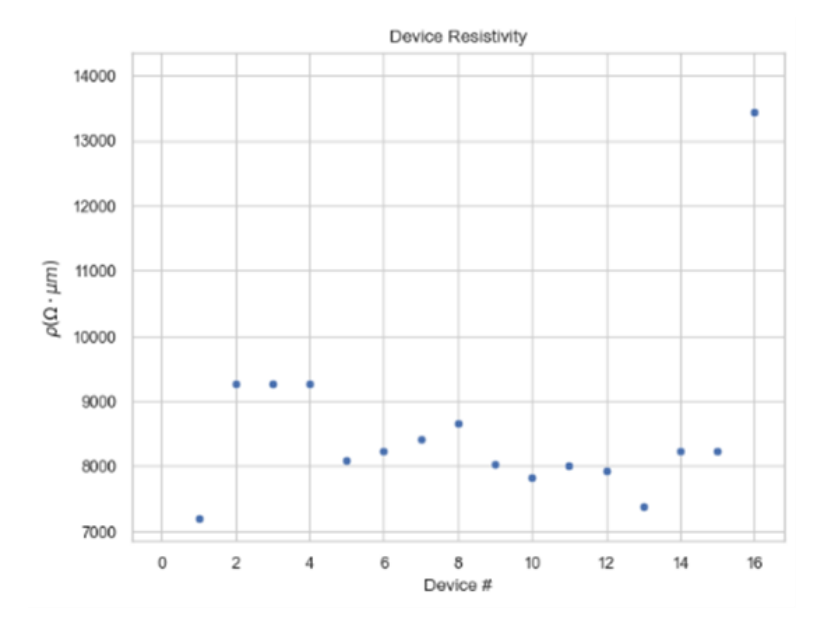


Figure 3.2: Measured resistivity of 16 printed resistors

The resistivity of 15 of the 16 resistors is around the cited value, but there is some significant deviation. This deviation could make it difficult to fabricate components with high degrees of precision. The 16<sup>th</sup> resistor is an outlier and is the result of a printing error.

To control the resistivity value more precisely, the curing profile was changed to match the curing profile of silver, 180°C for 5 hours. This curing profile was used during the fabrication of the 30 GHz power divider (section 4.2.2) since the resistor would be subjected to a

final silver cure. The hotter and longer cure did aid in increasing the precision of the resistivity values. Changing the curing profile both increased the precision of the resistor resistivity and lowered the average resistivity value. This will be beneficial for trying to make low resistance components. The results of the new curing profile on resistivity can be seen in figure 3.3.

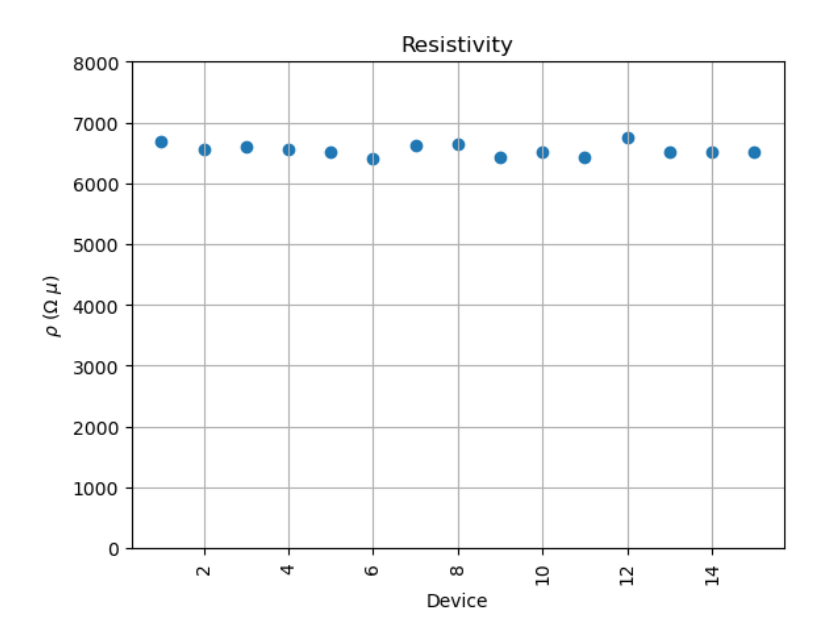


Figure 3.3: Component resistivity with long, hotter cure

A sample of the I-V curves for the printed resistor are given in figure 3.4. An ideal curve would be linear and increasing. This would show that the current through the resistor is directly and proportionally related to the voltage applied across the resistor. This is indicative of ohmic behavior; therefore, the resistor follows ohms law (equation 3.2).

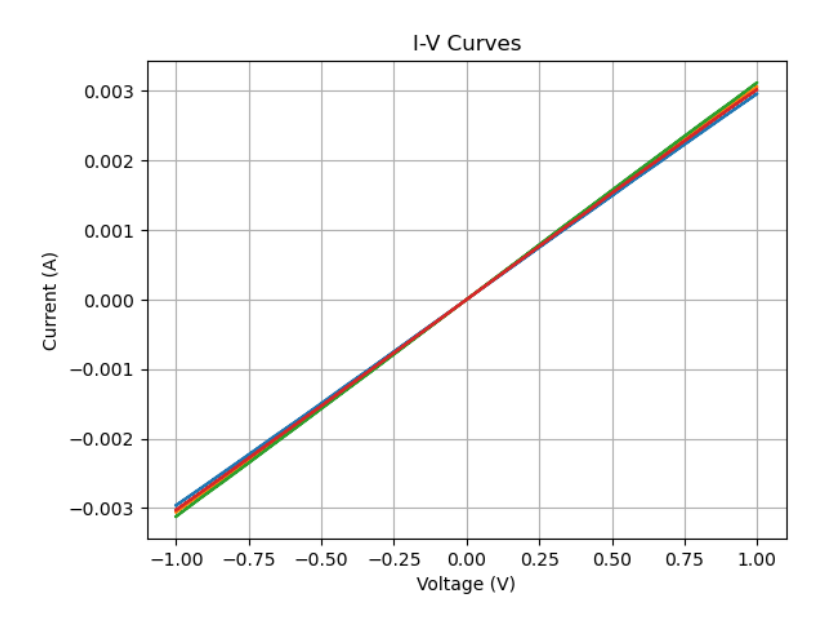


Figure 3.4: Device I-V curve

$$R = \frac{V}{I} \tag{3.2}$$

Equation 3.1 shows that the resistance of a device is determined by both the resistivity and cross-sectional area of the device. This can pose a problem during fabrication since the geometry of the device (cross sectional area) will change during cure as the solvent in the carbon ink is flashed off. This makes it important to understand how a given cure profile will affect the geometry of the printed device. With the curing profile established to be 180°C for 5 hours, the geometrical change in cross sectional area is shown for all sixteen devices in figure 3.5.

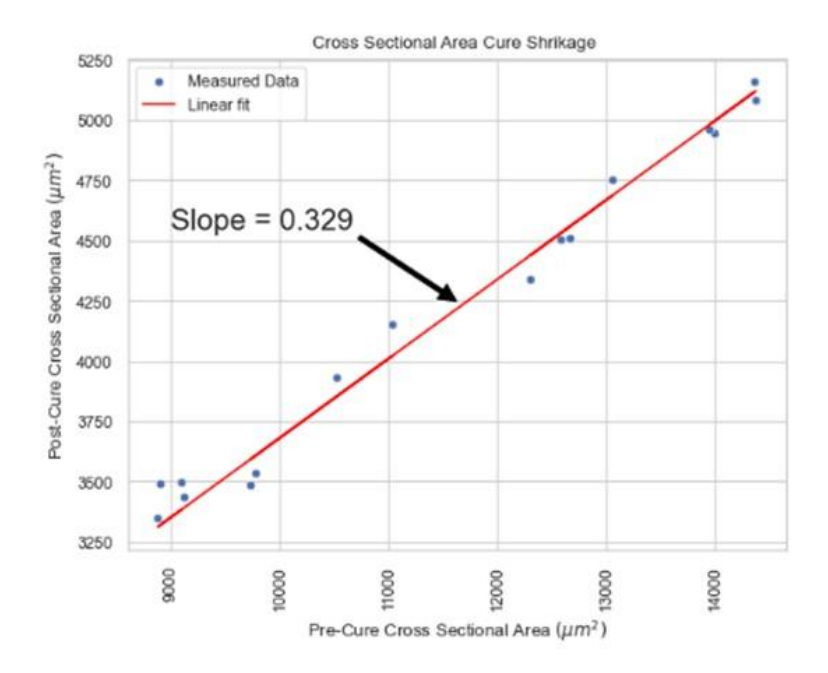


Figure 3.5: Change of resistor cross-sectional area due to cure

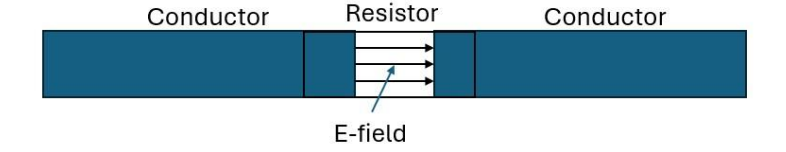
The amount that the resistor geometries change during the cure is relatively consistent and predictable. The slope of the linear line of best fit is a good approximation for how the resistor cross-sectional area changes during the cure. With this shrinkage profile, it is possible to modify equation 3.1 to give an equation that can be used to determine resistor geometry before cure. The benefit being that the user can get closer to desired resistance values with less print steps. The modified equation to account for the change in cross-sectional area is given in equation 3.3.

$$R = \rho \frac{0.3 \ length}{cross - sectional \ area} \tag{3.3}$$

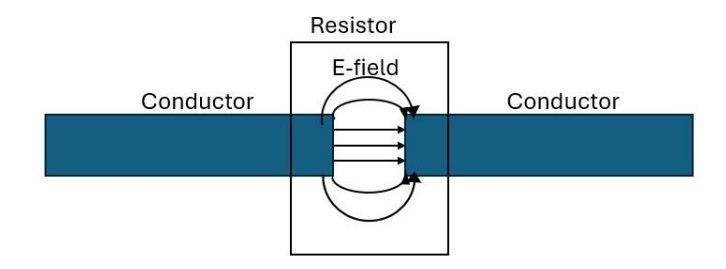
Note that the device length does not change, as this is determined by the separation of the silver conductors. Additionally, the resistivity does not change since that is a material property of the ink.

Equation 3.3 is an approximation and is only true when a given set of conditions are satisfied. The most notable of those conditions concerns the cross-sectional area of the resistor.

In equation 3.3 cross – sectional area = resistor width × resistor height, and there is a limit to how large either the width or height for a given device can be. Put into the extreme, the width can not be infinitely large or the height infinitely high and produce a device of  $0\Omega$  resistance. To prove this case, a microstrip was fabricated and numerous print runs were performed to build the height of the resistor to be extremely tall. The resistor was measured to have a resistance of  $147\Omega$ , then more layers were added on and measured again, the resistance was unchanged. This proved that there is an upper limit to the width and height. The conceptual reasoning behind this is shown in fig 3.6.



#### (a) Resistor with narrow width



(b) Resistor with large width

Figure 3.6: Electric field lines in different size resistors (conceptual)

To further prove this concept a simulation was run using Ansys HFSS to visualize the electric field in a printed resistor. The simulation is shown in figure 3.7. The red portion is the conductor. The green portions of the resistor are where the electric field is strongest, and the blue is where the electric field is the weakest. The electric field quickly dies off as distance from the conductor is increased.

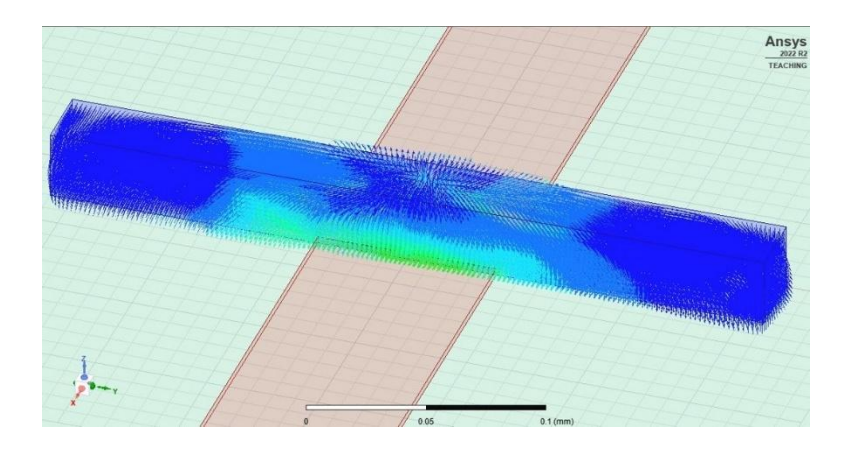


Figure 3.7: Electric field strength inside printed resistor

This shows that when the resistor width is narrow, the field lines from one conductor to the other are confined and utilize the entire width of the resistor. This forces the charge carries to move through the resistive material that constructs the entire resistor. In this case equation 3.3 is accurate; however, when the resistor has a large width the electric field lines do not use all the resistive material, and the charge carriers are not forced through the entire resistor. This makes the utilized width smaller than the physical width and equation 3.3 is no longer accurate. The same logic holds true for increasing the height of the device beyond a certain point. The observation made throughout this project is that if the height of the resistor is larger than the separation of the conductors, the I-V characteristics no longer behave as expected. The width of the resistor should not exceed 2 times the width of the conductors. These rules of thumb were discovered and used throughout; however, no rigorous experimentation was done.

# **CHAPTER 4: Fabricating RF Devices**

#### **4.1 Load Terminated Microstrip**

Terminated microstrip transmission lines play a large role in various RF circuits such as: hybrid couplers, quarter wave directional couplers, and rat race couplers. These examples represent four port devices where one port acts as an input port, two ports are outputs, and the final port is simply terminated with a matched load. These couplers typically offer a simple method to split/combine a signal and achieve various phase shifts. However, these devices can be constrained to lower frequencies if the load resistor is unable to be scaled to a small size. The goal for fabricating loaded microstrips was to determine whether it was possible to fabricate small resistors, and if possible, quantify its ability to absorb a signal and minimize reflections.

To understand the theory of operation, it will be assumed that the point where the microstrip meets the printed resistor is at x = 0. The signal is generated by a source that is located at some point before this point. Therefore, the signal is travelling from the source to the load in the +x direction, but at the microstrip to resistor interface, there will be some reflections that generate a wave travelling in the direction from the resistor back to the source. The sum of these waves gives the total voltage on the microstrip and is given in equation 4.1. The voltage is related to the current via the impedance using equation 4.2.

$$V(x) = V_0^+ e^{-j\beta x} + V_0^- e^{j\beta x}$$
(4.1)

$$I(x) = \frac{V_0^+ e^{-j\beta x}}{Z_0} - \frac{V_0^- e^{j\beta x}}{Z_0}$$
 (4.2)

The impedance of the load can be found by divider equation 4.1 by 4.2 at the point x = 0. This is given in equation 4.3.

$$Z_L = \frac{V(0)}{I(0)} = \frac{V_0^+ + V_0^-}{V_0^+ - V_0^-} Z_0$$
(4.3)

Finally, the reflection coefficient,  $\Gamma$ , can be determined by rearranging to find the ratio of the forward travelling signal and the backward travelling signal. The reflection coefficient can be found strictly in terms of the load and characteristic impedance. See equation 4.4.

$$\Gamma = \frac{Z_L - Z_0}{Z_L + Z_0} \tag{4.4}$$

Equation 4.4 shows that if the load impedance is well match to the characteristic impedance, reflections can be minimized. This can be highly desirable since reflections can result in poor performance of RF parts. Minimizing reflection also makes it possible to isolate the RF circuits from unwanted signals, as will be done when fabricating the V-band Wilkinson power divider in section 4.2.2.

Fabrication of the loaded microstrips started with mechanically removing the oxide on a molybdenum-copper (MoCu) carrier plate that is 1"x1" in size. This carrier plate acts as a stage onto which the AJP parts will be fabricated and will also act as the ground plane for the microstrip lines. Polyimide was deposited to serve as the dielectric substrate layer upon which the silver will be printed. The width of the silver to obtain a characteristic impedance of  $50\Omega$  was  $50\mu$ m, which is not wide enough to print a resistor that has an impedance that low for the reason that is shown in figure 3.5. To overcome this challenge, a small set of flanges were added either side of the resistor, a pictorial representation is shown in figure 4.1. It is important that these flanges remain small when compared to the wavelength, otherwise, they could have a negative effect of circuit performance when it begins to act as a distributed element. In this situation the flanges were made to be  $200\mu$ m long and  $40\mu$ m wide.



Figure 4.1: Microstrip flanges to increase resistor width

This process was repeated 12 times over to fabricate 12 individual microstrips. The resistors were then printed to a varying height with an increasing number of layers. For example, the first loaded microstrip only has a single layer of carbon printed for the resistor, the second microstrip has 2 layers of carbon, and the final loaded microstrip has 12 layers of carbon printed for its resistor. This resulted in a range of resistance values from as high as  $206\Omega$  to as low as  $45\Omega$ . The printed microstrip and its resistor is shown in figure 4.2, and the resistance measurement for each resistor is given in figure 4.3.

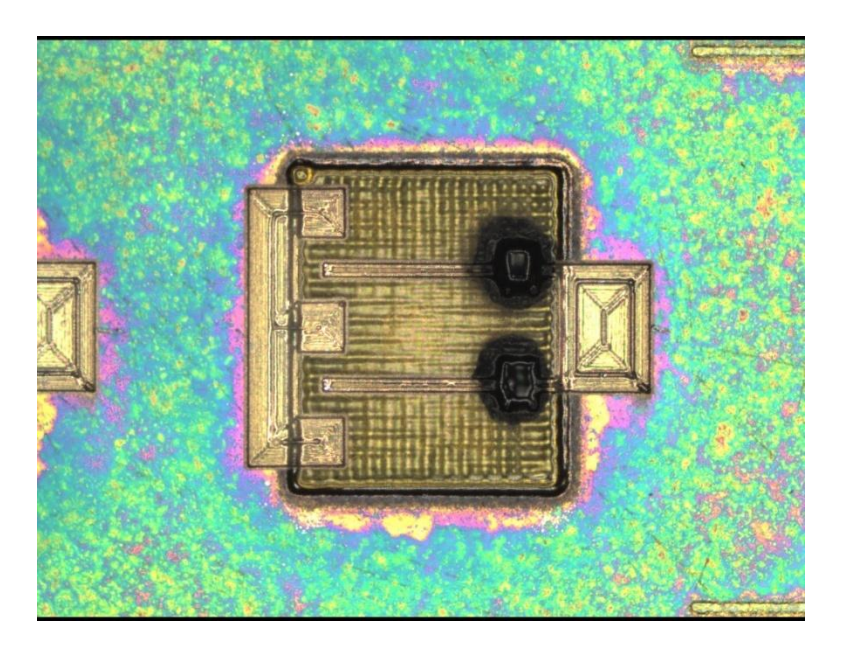


Figure 4.2: Two loaded microstrips

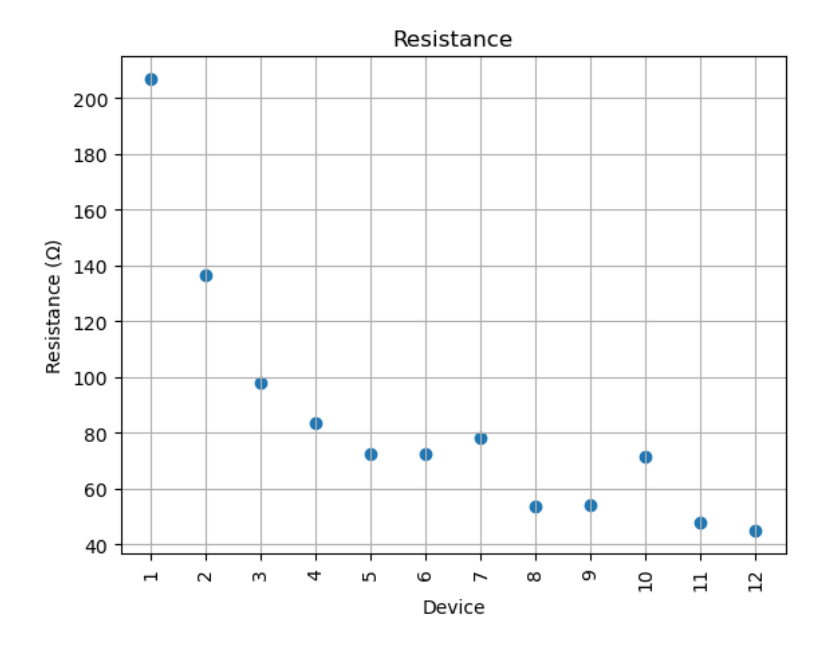


Figure 4.3: Resistance measurement of each loaded microstrip resistor

These microstrips were measured through W-band to determine how this device operates at both low and high frequencies. To convert equation 4.3 into something that can be directly measured, the reflection coefficient can be used to determine the return loss, which is directly measured. Equation 4.5 converts the reflection coefficient into a return loss.

$$RL = -20log(\Gamma)dB \tag{4.5}$$

Based on equations 4.3 and 4.4 it is expected that as the resistance of the printed resistor approaches the characteristic impedance, the return loss will improve. The measured DC resistance value, the calculated reflection coefficient, and the calculated return loss are given in table 4.1. These calculations were done using measured resistance as the load impedance. Figure 4.4 shows the measured results of all the loaded microstrips. Figure 4.5 compares four measured and simulated microstrips.

Table 4.1: Calculated return loss using measured resistance values

Device	$Z_{\mathrm{L}}$	$Z_0$	Γ	RL (dB)
1	206	50	0.61	4.3
2	136	50	0.46	6.7
3	98	50	0.32	9.8
4	83	50	0.25	12.1
5	72	50	0.18	14.9
6	72	50	0.18	14.9
7	78	50	0.22	13.2
8	53.	50	0.03	30.7
9	54	50	0.04	28.3
10	71	50	0.17	15.2
11	47	50	0.03	30.2
12	45	50	0.05	25.6

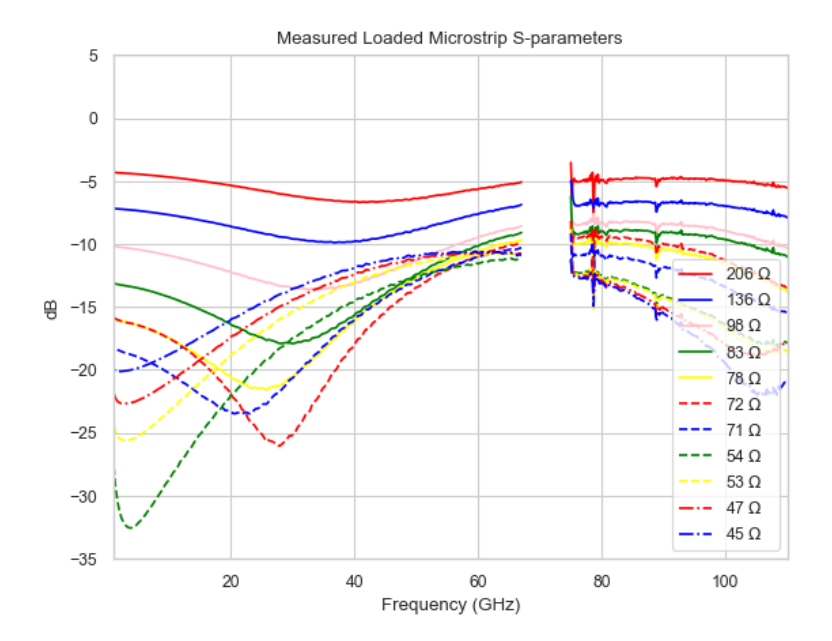


Figure 4.4: VNA measurements of the loaded microstrips

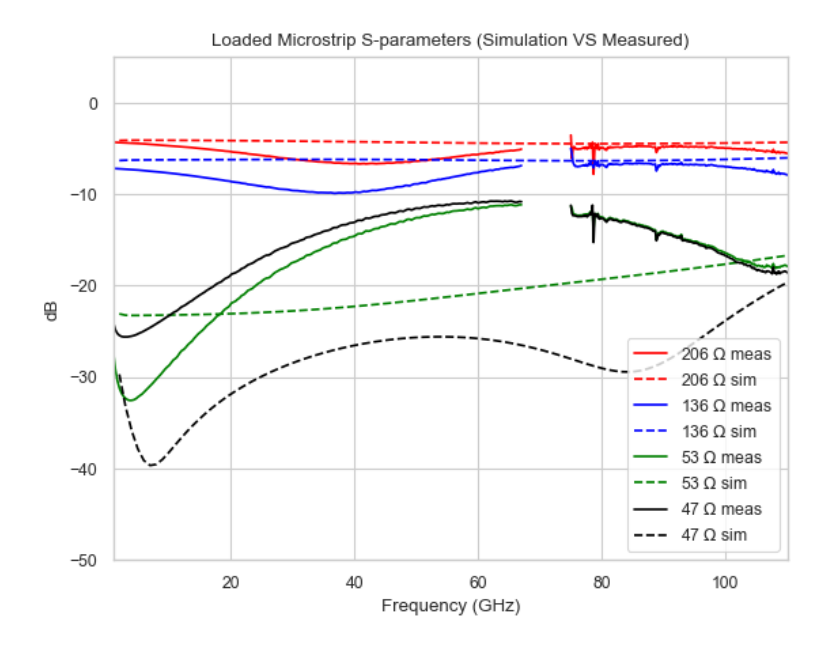


Figure 4.5: Measured VS Simulated loaded microstrips

In total, the loaded microstrips operate acceptably well when compared to the simulated values; however, the performance could be better. This degraded performance could be for a couple major reasons: The characteristic impedance is not perfectly  $50\Omega$ , the resistance of the printed carbon is changing at RF frequencies due to the skin effect, and parasitic inductance and capacitance may dominate in higher frequency ranges. Even with these potential issues, the return loss of the resistors that are within 5% of the characteristic impedance is better than 10 dB at all frequencies up to 110 GHz.

#### 4.2 Wilkinson Power Divider

# 4.2.1 Background/Theory

The Wilkinson power divider is an N-port device that is used to split power equally N-ways and was originally introduced in 1960 by E.J. Wilkinson [19]. In this divider two quarter wave transformers are connected to a common input port and two separate output ports. Separating the output arms of the power divider is an isolation resistor that has a value of  $2Z_0$ ,

where  $Z_0$  is the characteristic port impedance. The quarter wave transformer is used to impedance match the port with the isolation resistor and minimize the resulting reflections.

When power is incident on the input port it is equally split between each quarter wave transformer. Since the device is symmetrical, when the signal reaches the resistor both arms have a signal that is equal in both phase and magnitude, therefore, there is no potential difference across the resistor and current does not move through it. Each output port would receive half the power and measure at roughly -3dB. In this case, the device is acting as a divider. If two signals that were equal and in phase where incident on the output ports, the device would have the same operation in reverse and would be acting as a combiner.

When power is incident on a single output port that signal travels through two quarter wave transformers to reach the opposite output port, therefore, the signal has a phase offset of 180 degrees across the resistor. This corresponds to the largest potential across the resistor and as a result the largest current through the resistor. The power being consumed inside the resistor is in accordance with P = IV and isolates the output ports from each other.

The resistor plays a large role in the performance of the Wilkinson power divider and its ability to isolate signals and reflection. For this reason, a Wilkinson power divider was chosen to act as a test bed for the printed resistor.

#### 4.2.2 Ka-Band Wilkinson Power Divider

The Wilkinson power divider has port impedance of  $50\Omega$ , this value is chosen since it is both industry standard and is the port impedance of the PNA-X that was used to measure its performance. The resistor separating the output arms was  $100\Omega$ . To ensure that the resistor did operate as a lumped element device its largest aspect ratio was kept to less than one-tenth the wavelength. The wavelength of the signal can be calculated using equations 4.6 and 4.7 [20].

$$\epsilon_e = \frac{\epsilon_r + 1}{2} + \frac{\epsilon_r - 1}{2} \frac{1}{\sqrt{1 + 12\frac{d}{w}}} \tag{4.6}$$

$$\lambda = \frac{c}{f\sqrt{\epsilon_e}} \tag{4.7}$$

The dielectric for the divider is made from PI-2611, manufactured by HD microsystems, diluted with N-Methyl-2-Pyttolidone (NMP) at a ratio of 2:3 by volume. The dielectric constant for this dielectric mixture has been found experimentally to be roughly 3.5. This is consistent with other works done that used similar materials [21]. The conductor used for the power divider is Clariant silver ink diluted with distilled water at a ratio of 1:3 by volume, respectively. It has been found that this mixture after cure has a conductivity,  $\sigma$ , in the range of 20% - 40% the conductivity of bulk silver.

The narrowest portion of the silver traces was along the quarter wave transformer. This portion of the conductor was the limiting factor that helps determine the height of the dielectric, since the dielectric height directly affects the microstrip width needed to achieve a given impedance value. The impedance along the quarter wave transformer was  $\sqrt{2Z_0}$ , or  $70.7\Omega$ . The design equations used to determine the ratio between the width of the microstrip line and the height of the dielectric are given in equations 4.8 and 4.9. Both can be found in [20]. These equations are only valid when  $\frac{W}{d} > 2$ , which will be the case for this device.

$$B = \frac{377\pi}{2Z_{0\sqrt{\epsilon_r}}}\tag{4.8}$$

$$\frac{W}{d} = \frac{2}{\pi} \left[ B - 1 - \ln(2B - 1) + \frac{\epsilon_r - 1}{2\epsilon_r} \left( \ln(B - 1) + 0.39 - \frac{0.61}{\epsilon_r} \right) \right]$$
(4.9)

Based on the above equations, the target height for the dielectric was chosen to be roughly 40µm. This dielectric height would result in a theoretical trace width of 108µm and

 $64\mu m$  for a characteristic impedance of  $50\Omega$  and  $70.7\Omega$ , respectively. These widths were optimized in HFSS, and the target widths will be  $100\mu m$  and  $50\mu m$ , which is near the theoretical values.

To determine the maximum allowable size of the resistor the wavelength must be known. The wavelength of the signal can be found using equation 4.10, 4.11 [22].

$$v_p = \frac{1}{\sqrt{\epsilon_0 \epsilon_r \mu}} = \frac{c}{\sqrt{\epsilon_e}} \tag{4.10}$$

$$\lambda = \frac{v_p}{f} = \frac{c}{\sqrt{\epsilon_e f}} \tag{4.11}$$

This yields a wavelength of 4.4mm. One-tenth of this is 0.44mm or 440 $\mu$ m, which is the largest that the resistor should be. This is well within the capabilities of the AJP process. The final resistor dimensions are 250 $\mu$ m  $\times$  100 $\mu$ m. The HFSS model of the Wilkinson power divider is given in fig 4.6.

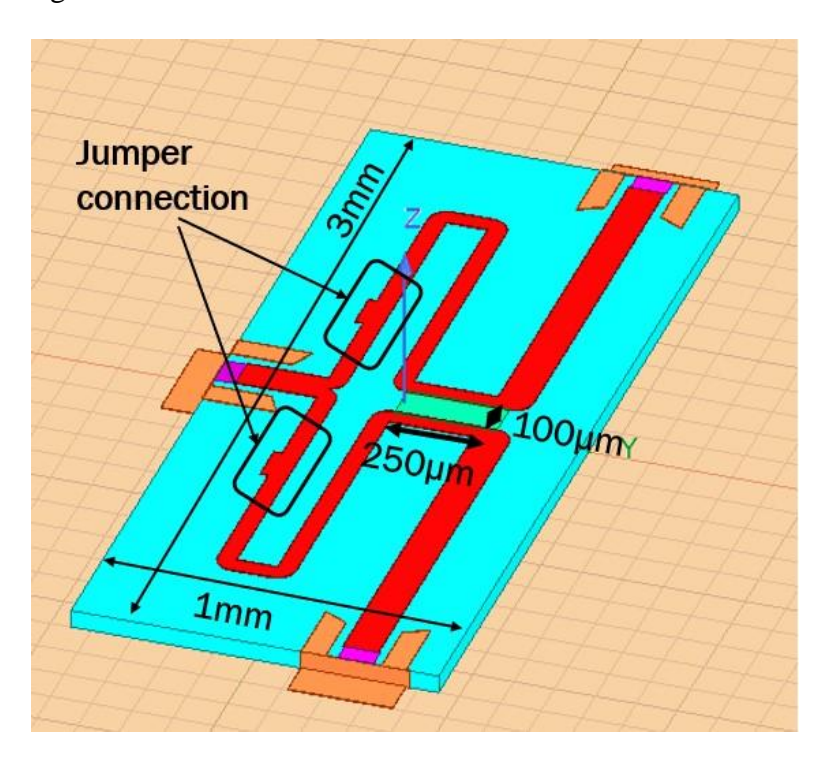


Figure 4.6: HFSS model of Ka-band Wilkinson power divider

A molybdenum-copper (85% molybdenum and 15% copper) carrier plate is used as the ground plane. This mixture of MoCu is used to match the coefficient of thermal expansion of group III-V semiconductors (this is not a concern for this device and any good conductor would have been sufficient). The carrier plate was mechanically sanded and polished using a Dremel and sanding disks up to 10000 grit. The sanding process helps remove any surface oxide and preps the surface for the application of adhesion promoter. The adhesion promoter is 0.1% VM-651, manufactured by HD Microsystems) diluted with 99.9% deionized water. The adhesion promoter is used to ensure the polyimide substrate adheres strongly to the ground plane and minimizes the chance of delamination during the curing steps. polyimide was applied in 10µm thick layers using the pneumatic atomizer. The recipe for this print consisted of a sheath gas mass flow rate of 80 SCCM, 800 SCCM pneumatic atomizer mass flow rate, 775 SCCM exhaust mass flow rate, a 300 $\mu$ m tip and speed of 1  $\frac{mm}{s}$ The part then placed on a hot plate to soft bake up to 200°C. The soft bake help flash off solvents in the polyimide in the bottom layers prior to adding further layers. This minimizes the potential for delamination and bubble formation in the substrate. The final hard cure was 300°C for three hours. The final dielectric height was 41.5µm (not accounting for surface roughness). The measurement results are given in Fig 4.7.

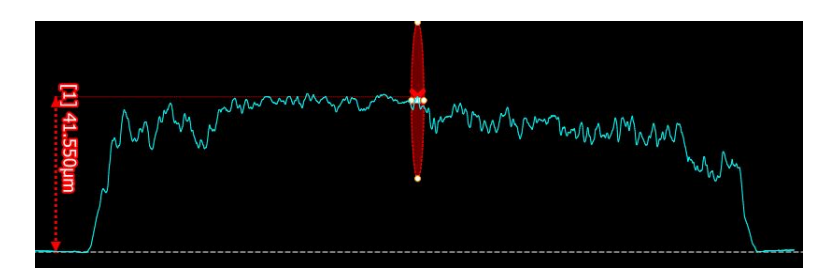


Figure 4.7: Polyimide height measurement

To minimize the electrical losses in the silver, the target thickness of the silver is chosen to be multiple times larger than the skin depth. The skin depth can be calculated using equation

4.12 [22].

$$\delta = \sqrt{\frac{2}{\omega\mu\sigma}} \tag{4.12}$$

Where  $\omega$  is the frequency of the signal in radians per second,  $\mu$  is the conductivity or permeability of silver, and  $\sigma$  is the conductivity of silver( $\omega=2\times\pi\times$  freq,  $\mu=4\times\pi\times10^{-7}\times0.9998$ ,  $\sigma=6.173\times10^{7}\times0.2$ ). This gives a skin depth of 0.8 $\mu$ m. The skin dept represents the value at which a signal is attenuated to  $\frac{1}{e}$  of its initial value. The thickness of the silver should be at least three times this value. The silver was deposited using the ultrasonic atomizer with a recipe of 75 SCCM sheath gas flow, 30 SCCM ultrasonic atomizer flow, \$200\mu m\$ tip and tip speed of  $1\frac{mm}{s}$ . All silver cures were subject to a hard cure of  $180^{\circ}$ C for 5 hours. The measurement results for the silver are given in figure 4.8.

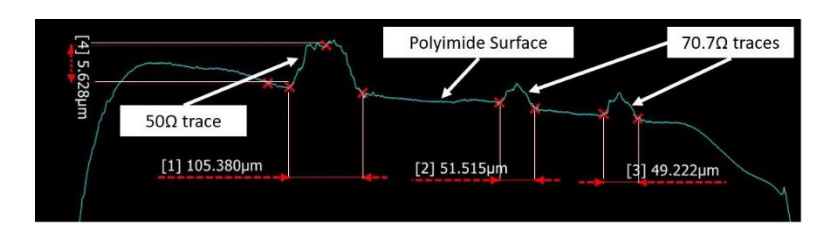


Figure 4.8: Ka-band divider silver measurement

The silver thickness is much more than the needed  $2.4\mu m$ . The widths of the  $50\Omega$  and  $70.7\Omega$  traces are  $105\mu m$  and either  $51\mu m$  or  $49\mu m$ , these correspond to values within 5%. A gap was left in the quarter wave transformer during the initial silver print. This gap allows for measurement of the isolation resistor during fabrication. The power divider at this point in fabrication is given in figure 4.9.

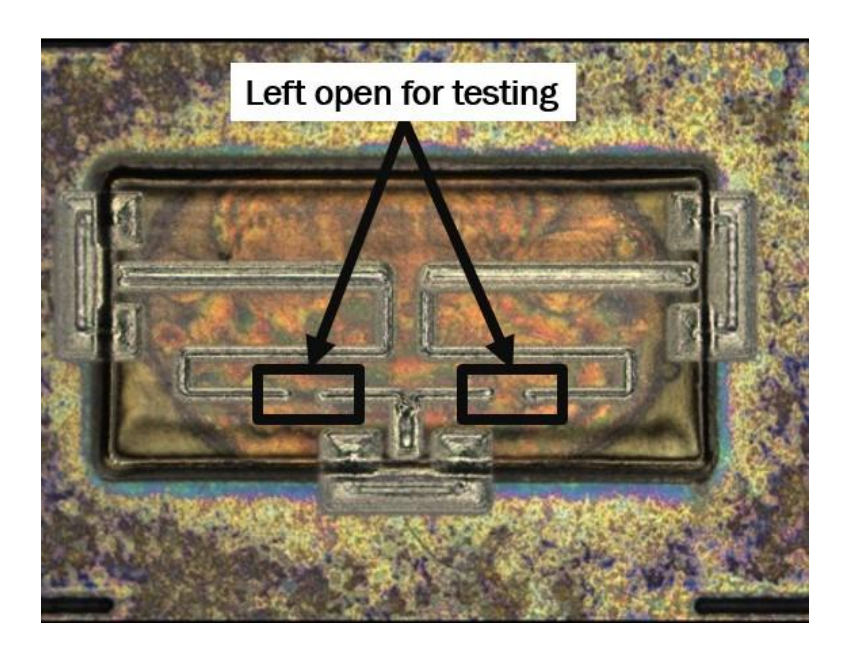


Figure 4.9: Ka-band divider prior to resistor fabrication

The isolation resistor was fabricated in four stages. Following each stage the resistor was value was measured using a 4-point probe. The first stage was printed to an arbitrary height, then measured. This made it possible to ensure that the resistor properties, resistivity, and resistance, were tracking as expected during fabrication. The following three stages were printed with the intention of getting closer to the desired resistance value ( $100\Omega$ ) without going under. Between each print step the part was cured in  $180^{\circ}$ C for five hours. This curing profile was selected because it is the curing profile of silver, and a final silver cure would still be needed to connect the quarter wave transformer. Curing the carbon at these temperatures helped ensure that the carbon ink could mechanically withstand these temperatures as well as minimize unwanted additional cures during the silver cure that connects the quarter wave transformers together. The carbon print recipe was as follows: 75 SCCM sheath gas flow, 25 SCCM ultrasonic atomizer flow,  $200\mu$ m tip, and a speed of  $1\frac{mm}{s}$ . Following resistor fabrications, the quarter wave transformers were connected with a silver jumper. The divider following the resistor fabrication is given in figure 4.10. The measured resistance values between each print stage are given in

figure 4.11. The measured resistivity values between each print state is given in figure 4.12.

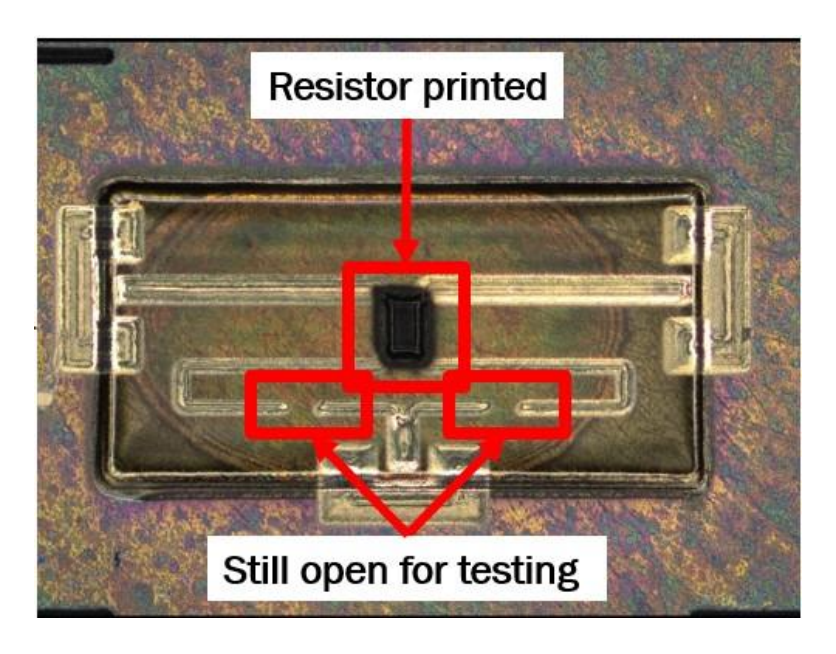


Figure 4.10: Ka-band divider after resistor fabrication

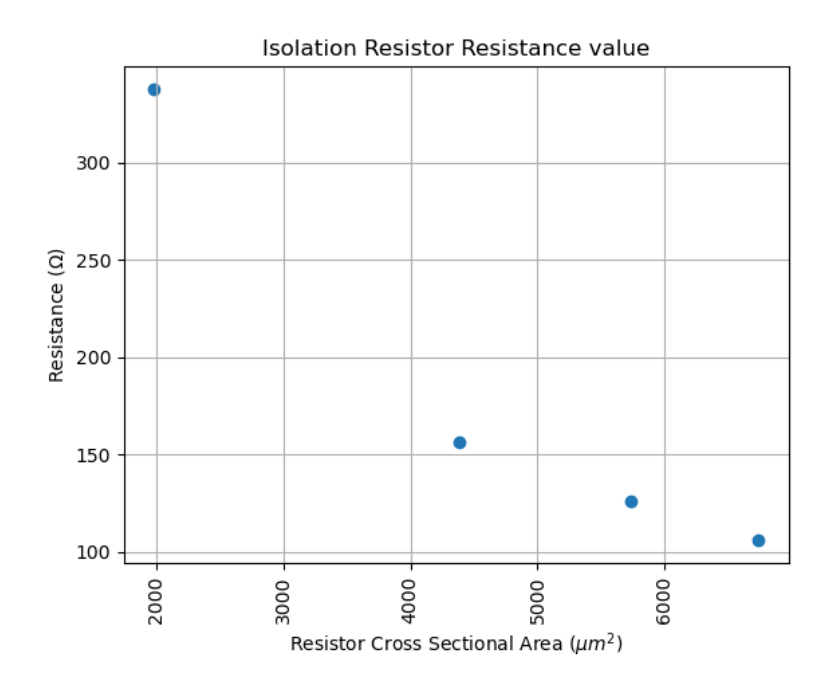


Figure 4.11: isolation resistor resistance values during fabrication

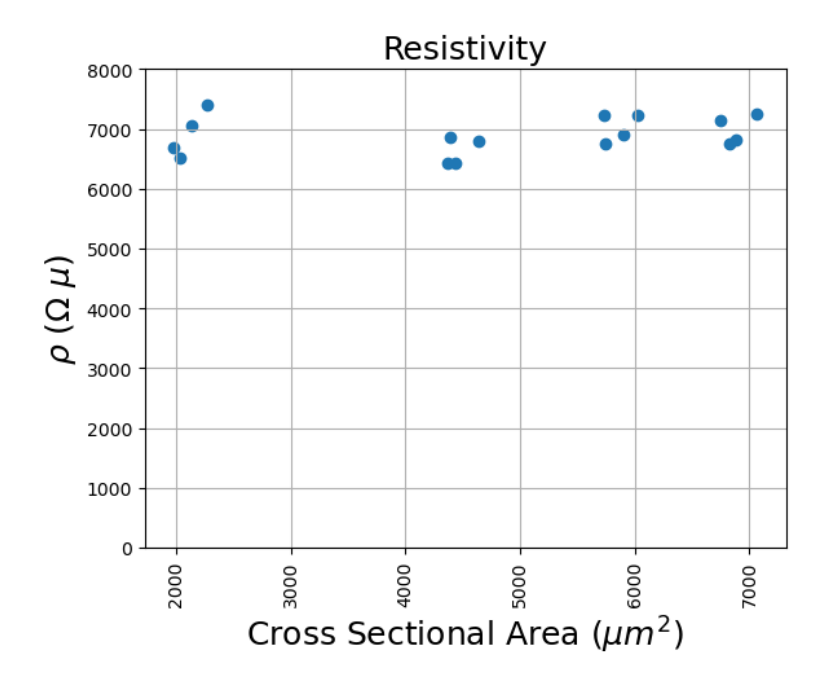


Figure 4.12: Resistivity of isolation resistors during fabrication

The resistance value drops as the cross-sectional area is increased; however, the resistivity remains relatively constant regardless of cross-sectional area. This is the expected behavior of the resistive ink. It is simple to add more ink, but no good method of ink removal was tested, this is why multiple steps were used. The final resistance value was  $106\Omega$ , which is within 10% of the theoretical value. Additionally, this resistor is  $250\mu m$  wide and  $100\mu m$  long. This is smaller than available packaged thick film resistor and removes the requirement to mount a thin film resistor. This Wilkinson power divider was made homogeneously using aerosol jet printing, no additional forms of manufacturing or external parts were needed. The completed Wilkinson power divider is shown in Fig 4.13.

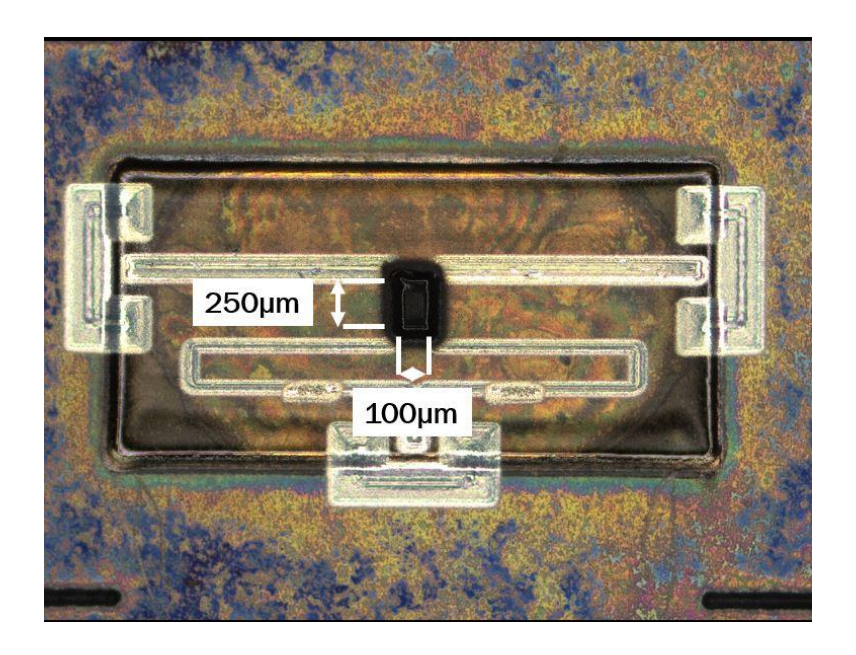


Figure 4.13: Completed Ka-band Wilkinson power divider

The power divider was then tested using three ground-signal-ground (GSG) probes, manufactured by GGB Industries INC, and a 4-port network PNA-X manufactured by Keysight (N5245B). The network analyzer was calibrated using a short-open-load-transmit (SOLT) method on a CS-5 calibration substrate. This brings the reference plane to the probe tips. Because the three ports were measured simultaneously, 90-degree bends on the calibration substrate were used for the thru standard between ports 1 and 2 and ports 1 and 3. The measurement results are given in Fig 4.14.

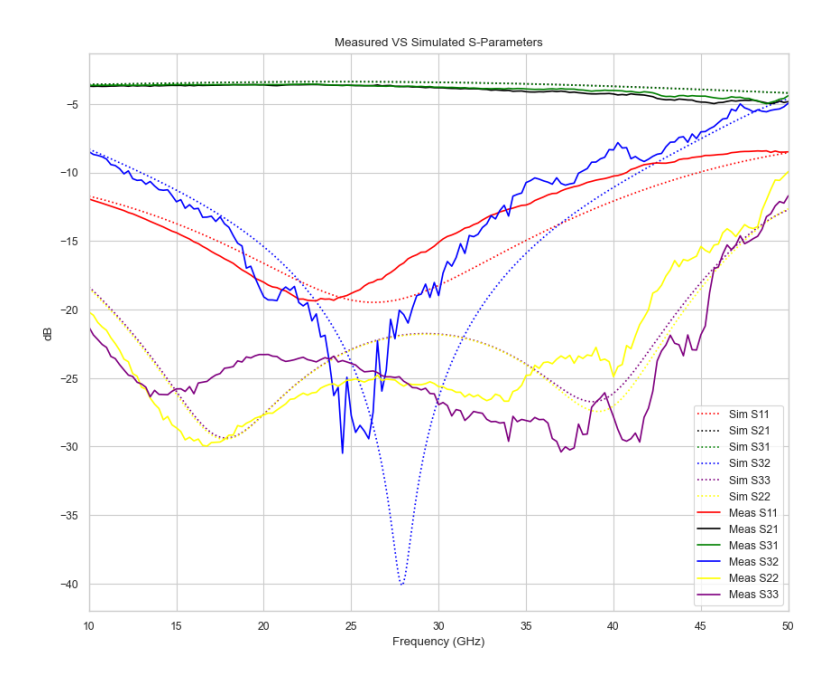


Figure 4.14: Ka-band Wilkinson power divider results

Measurements show that the power divider operates within common performance limits across a range of 15-35 GHz. Within that range, the input match ( $S_{11}$ ) is below -10 dB, the output port isolation ( $S_{32}$ ) is below -10 dB. The output port isolation is related to the performance of the printed isolation resistor.  $S_{22}$  and  $S_{33}$  are less than -20 dB in this range. The added insertion loss is less than 0.7 dB beyond the nominal 3 dB power splitting in the 15-25 GHz range and less than 0.9 dB from 15-35 GHz. The output ports are well balanced with less than 0.1 dB difference between  $S_{21}$  and  $S_{31}$  at a given frequency. This proves the effectiveness of the printed resistor in a common RF component for applications at least up to Ka band.

### 4.2.3 V-Band Wilkinson Power Divider

A V-band Wilkinson power divider was fabricated using the same method that was used to fabricated the Ka-band power divider with one notable expectations. This difference concerns how the part would be measured. It is possible to measure all three ports of the Ka-band Wilkinson simultaneously; however, this would not be possible with the equipment available

when attempting to measure in V-band, so a method was needed to convert a three-port device into a two-port device. This transformation was done by fabricating two separate devices and placing a load resistor at one of the ports. One of the dividers terminated an output port, this allowed for measurements to be taken for  $S_{11}$  and  $S_{21}$ . The other divider would have the input port terminated to allow for measurements of  $S_{32}$ , the amount of isolation between the output ports. These measurements were then combined to interpolate the performance of a single device with no terminated ports. The V-band Wilkinson power divider is shown in figure 4.15.

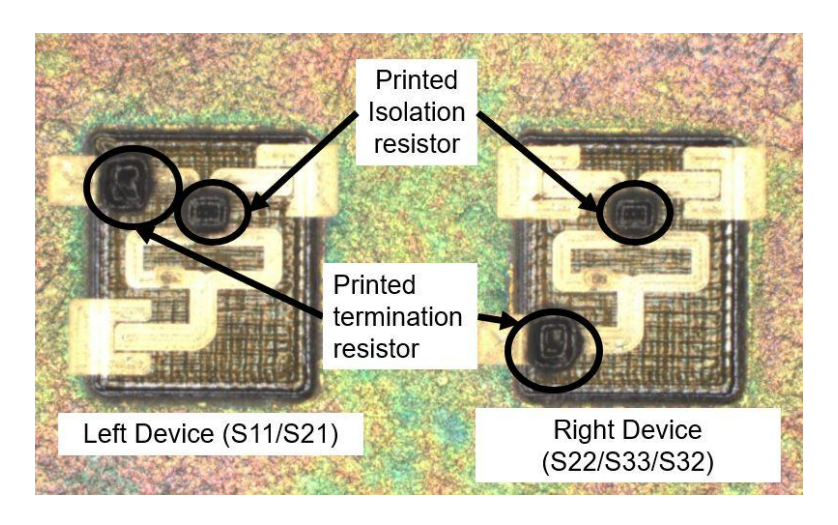


Figure 4.15: Both halves of V-band Wilkinson

The left termination, right termination, left isolation, and right isolation resistors have values of  $80\Omega$ ,  $76\Omega$ ,  $113\Omega$ , and  $115\Omega$ , respectively. The isolation resistor values are within 15% of the desired  $100\Omega$  and should not affect the performance of the divider significantly, and any degradation in performance due to this would be observed as a degradation in output port isolation ( $S_{32}$ ). The left and right termination resistors are off their target of  $50\Omega$  by about 60 and 52 percent, which does have the potential to significantly impact the device performance; however, as can be seen in figure 4.4, the return loss at these resistance values is slightly larger than 10 dB. This corresponds to nearly 90 percent of the signal getting attenuated, then in the case of the left device, that signal is further attenuated by the isolation resistor. This combination

ensured that while the resistor values are far from their target, they will still be functional and makes the risk of additional heat cycles not worth attempting. The performance of the V-Band power divider is given in figure 4.16.

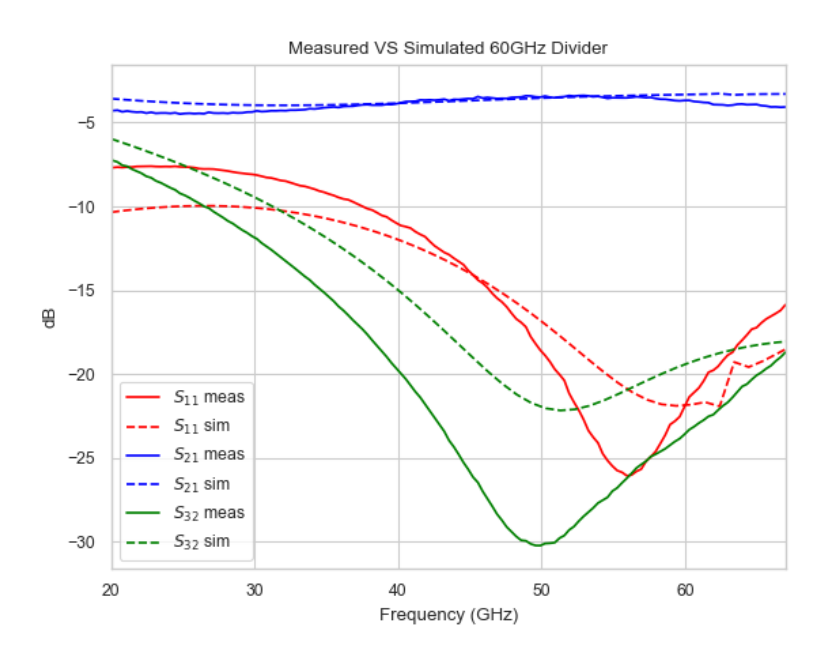


Figure 4.16: Measured and simulated results of V-band power divider

This V-band power divider a high degree of isolation, S<sub>32</sub> is less than -15 dB, starting at 35GHz and continuing up to at least 67GHz. Any disturbance and/or reflection that occur at one of the output ports will have a small effect on the opposite output port. The return loss is low, more than 15 dB, at and above 45 GHz up to at least 67 GHz. Therefore, more than 97% of the power that is incident on the input port is transmitted into the system. The insertion loss for this system is 1 dB larger than the ideal 3 dB split in the frequency range 37.2 - 65.3 GHz. The insertion loss improves to being within 0.5 dB when the frequency range is further restricted to 45.6 - 58 GHz.

# **CHAPTER 5: Conclusions and Future Work**

It was shown in this thesis that using commercially available carbon black ink can be used in the AJP process. The ink was characterized to determine its resistivity and geometrical properties. Knowing the resistivity value is what will give engineers the ability to customize the resistor value and geometry to the needs of a given application. An additional understanding of how the resistor changes during cure will allow those using AJP to print resistors reliably and with fewer tuning steps. This thesis has also shown that these printed resistors can be used in RF components and their effectiveness was shown up to V-band. Practical termination resistors were shown effective through W-band. This could have significant practical uses in both component fabrication and packaging as the world moves to utilize higher regions of the RF spectrum.

While this thesis was a step in the right direction to prove the effectiveness of printing resistors, some work remains.

# **5.1 Altering Ink Resistivity**

Resistor size was a significant obstacle throughout the course of this work. The best method that existed to decrease the resistance value of a given device was to attempt to increase height and/or increase the device width. It would be beneficial if there was a method to lower the resistivity of the ink. This could potentially be done in a few ways.

Experiment with the curing process to see if there is a recipe that would lower resistance further without damaging the device. It was shown in chapter 3 that converting from the 100°C 30-minute cure to the 180°C 5-hour cure did lower the resistivity value, but no work was done to find the optimal curing profile. The environment (atmosphere) that the resistors were cured in was never changed. While it was uncommon, there were instances where the resistive ink would crack during the curing process. Placing the device under vacuum during cure may help remove

excess air from the ink prior to the ink hardening. Removing this access air may help prevent cracking as well as make resistor less porous, leading to a lower resistivity.

At no point in the course of this work was the ink recipe altered. It may be possible to add certain materials to the ink to change the ink's carbon-solvent ratio. Future work could focus on introducing water to the ink to lower the carbon-water ratio of the ink. This could lower the amount of carbon deposited using the same print while also lowering the viscosity and enabling more precise printing. Additionally, this work could be expanded past water and include studies on adding other materials with different resistivity values, such as adding small amounts of highly conductive ink. It is possible that mixing in lower resistivity materials may help lower the overall resistivity; however, it is also possible that small channels consisting of low resistivity materials form and bypass the less conductive ink.

## **5.2 Power Testing**

Power testing the resistor would be beneficial. If the power handling capabilities of the ink were known, the limits of what is possible with the ink would similarly be known. This would be difficult given that power handling is heavily affected by resistor size and resistor size is variable using this fabrication process. The power testing would need to be done both at DC and RF. While this thesis did prove that the printed resistors worked in RF circuits, the power levels were extremely low. DC testing of the device was normally kept between -1 and 1 volt, and never more than 20mA across the resistor.

### **5.3 Additional Circuits**

It would be beneficial to use this process in additional circuits to further test the abilities of the printed resistors. Devices such as attenuators could be made. Given that the resistance can be fabricated as desired, the resistance value can also be tuned, operators are no longer confined

to commercially available values. This could make attenuators that have attenuation values from 0dB all the way to complete attenuation. Additionally, having the ability to control resistance could help fabricate resistive power dividers with various power splitting ratios.

Fabricating termination resistors was also possible. This could have wide ranging uses in any device that requires termination resistors such as branch line couplers, rat race splitters, and terminated transmission lines.

#### **WORKS CITED**

- [1] X. Konstantinou, X. Lan, N. K. A. Escorcia, R. Sandhu, J. Tice, W. Spain, J. Albrecht and J. Papapolymerou, "Fully Aerosol Jet-Prited Passive Components for 140-220-GHz Operation," 2023.
- [2] F. Cai, Y.-h. Chang, K. Wang, K. W. T. P. S. and J. Papapolymerou, "High resolution aerosol jet printing of D- band printed transmission lines on flexible LCP substrate," in 2014 IEEE MTT-S International Microwave Symposium, 2014.
- [3] K. Grammer, J. Albrecht, P. Chahal, M. Hodek and J. Papapolymerou, "Low-Power Charactrization and Integration of Carbon Black Resistive Ink for Aerosol Jet-Printed RF Components," *IEEE Microwave and Wireless Technology Letters*, 2025.
- [4] X. Konstantinou, M. T. Craton, J. D. Albrecht and J. Papapolymerou, "Ultra-Wideband Transmission Lines on Complex Structures via Extendable Aerosol Jet 3D-Printing," in *IEEE International Conference on Microwaves, Antennas, Communications and Electronic Systems (COMCAS)*, 2021.
- [5] M. Craton, *MICROWAVE AND MILLIMETER WAVE SYSTEM INTEGRATION*, East Lansing, 2020.
- [6] N. Sturim, M. Hodek, P. Chahal, J. Albrecht and J. Papapolymerou, "High Density Multi-Layer Millimeter-Wave Packaging and Interconnects Using Aerosol Jet Printing," in *53rd European Microwave Conference (EuMC)*, 2023.
- [7] J. Navratil, K. Sima, T. Rericha and A. Hamacek, "Preparation and Application of Carbon Nanotubes Ink for Aerosol Jet Printing System," in 45th International Spring Seminar on Electronics Technology (ISSE), 2022.
- [8] J. Feng, A. Loveland and M. Renn, "Aerosol Jet Direct Writing Polymer-Thick-Film Resistors for Printed Electronics," *SMTA Journal*, vol. 34, no. 1, pp. 24-31, 2021.
- [9] M. T. Craton, C. Oakley, J. D. Albrecht, P. Chahal and J. Papapolymerou, "Fully Additively Manufactured Broadband Low Loss High Frequency Interconnects," in *Asia-Pacific Microwave Conference (APMC)*, 2018.
- [10] J. Howard and M. Graham, High Speed Digital Design: A Handbook of Black Magic, Pearsons, 1993.
- [11] i. Optomec, Aerosol Jet Depostion System Manual, 2011.
- [12] Herauses, Clevious FE T, HEP NTD TS ed., 2023.

- [13] X. Lan, X. Lu, T. Blumenthal, V. Fratello, W. Chan, M. Truong, K. Kiyono, Y. Zhang, G. Gu and M. Tan, "Ultra-wideband microwave components fabricated using low-cost aerosol-jet printing technology," *IEEE Radio and Wireless Symposium*, pp. 156-158, 2015.
- [14] W. Hartnell, J. Nguyen, L. Francis and D. Frisbie, "Self-aligned, inkjet-printed resistors on flexible substrates with excellent mechanical stability, high yield, and low variance," *Flexible and Printed electronics*, vol. 9, no. 2, 2024.
- [15] A. T. Erozan, R. Bishnoi, J. Aghassi-Hagmann and M. B. Tahoori, "Inkjet-Printed True Random Number Generator based on Additive Resistor Tuning," in *2019 Design*, *Automation & Test in Europe Conference & Exhibition (DATE)*, 2019.
- [16] N. Sankir, "Selective deposition of PEDOT/PSS on to flexible substrates and tailoring the electrical resistivity by post treatment," *Circuit World*, vol. 34, pp. 32-37, 11 2008.
- [17] S.-P. Rwei, Y.-H. Lee, S. J.-W. and U.-T. Shyr, "Characterization of Solvent-Treated PEDOT:PSS Thin," *Polymers*, 2019.
- [18] Novacentrix, Metalon JR-038 Datasheet, 2022.
- [19] E. Wilkinson, "An N-Way Hybrid Power Divider," *IRE Transactions on Microwave Theory and Techniques*, vol. 8, no. 1, pp. 116-118, 1960.
- [20] D. Pozar, Microwave Engineering, 4th ed., Wiley, 2011.
- [21] G. Ponchak and A. Downey, "Characterization of thin film microstrip lines on polyimide," *IEEE Transactions on Components, Packaging, and Manufacturing Technology: Part B*, vol. 21, no. 21, pp. 171-176, 1998.
- [22] R. Harrington, Time-Harmonic Electromagnetic Fields, Wiley, 2001.